Sciencexpress Report

Unraveling the Mystery of Indian Monsoon Failure During El Niño

K. Krishna Kumar,[1] Balaji Rajagopalan,[2,3] Martin Hoerling,[4]* Gary Bates,[4] Mark Cane[5]

[1]Indian Institute of Tropical Meteorology, Pune, 411008, India. [2]Department of Civil Environmental and Architectural Engineering, University of Colorado, Boulder, CO 80309, USA. [3]Cooperative Institute for Research in Environmental Sciences, University of Colorado, Boulder, CO 80309, USA. [4]NOAA Earth System Research Laboratory, Boulder, CO 80305, USA. [5]Lamont-Doherty Earth Observatory, Columbia University, Palisades, NY 10964, USA.

*To whom correspondence should be addressed. E-mail: martin.hoerling@noaa.gov

The 132-year historical rainfall record reveals that severe droughts in India have always been accompanied by El Niño events. Yet, El Niño events have not always produced severe droughts. We show that El Niño events with the warmest sea surface temperature (SST) anomalies in the central equatorial Pacific are more effective in focusing drought producing subsidence over India than events with the warmest SST in the eastern equatorial Pacific. The physical basis for such different impacts is established using atmospheric general circulation model experiments forced with idealized tropical Pacific warmings. These findings have significant implications for Indian monsoon forecasting.

Climate is the decisive influence on habitation and subsistence of India's burgeoning population. India's wealth is measured by its agricultural output, and now even modest harvest failures result in exaggerated economic and societal consequences. Swings in crop abundances are propelled by the year-to-year successes of the summer (June to September) monsoon rains (*1*). As a result, monsoon predictions are achieving new importance for setting into motion timely and effective preparedness and mitigation activities. Ironically, the predictions themselves can be as influential as the actual verified monsoon rainfall, as happened for Zimbabwe during 1997 when drought predictions led to curtailment of bank loans for agricultural development (*2*). A similar situation, also during 1997 occurred in India when a much touted prediction of poor monsoon rains proved false. A more painful scenario unfolded during 2002 and 2004 (*3*, *4*) when normal monsoon rains were predicted but severe drought materialized for which no contingencies were in place.

In many seasonal forecast tools Indian monsoon rains are predicted to vary in direct proportion to the strength of the El Niño Southern Oscillation (ENSO) phenomenon in the tropical Pacific (*5*–*7*), measured, for example, by the standardized NINO3 index (*8*). And, indeed, years with moderate to extreme cold states (NINO3 index < –1), have had abundant monsoon rains without exception. On the other hand, years of moderate to extreme warm states have not been reliably dry. As seen in Fig. 1, the 6 leading droughts (*8*) since 1871 have occurred in tandem with a standardized NINO3 index exceeding +1, but the presence of El Niños has not guaranteed drought. No simple association describes the relation between the Indian monsoon and NINO3 SSTs when moderate to strong El Niño conditions exist. Indeed, almost a full range of monsoon rains have accompanied SST warmings. For example, 1997 was the century's strongest El Niño, though no drought occurred, while the moderate El Niño of 2002 was accompanied by one of the worst Indian droughts of the past century (*4*). Such ambiguity undermines the utility of monsoon predictions used for mitigation of drought's societal impacts.

Two hypotheses are examined to understand this ambiguity in the El Niño–Indian monsoon relationship. One is that chaotic variability in rainfall on intraseasonal time scales masks the remote effect of El Niño. Accordingly, the failure (abundance) of monsoon rains during 2002 (1997) would be viewed as the accidental behavior of an inherently noisy monsoon system, and the poor forecasts for these particular cases were the consequence of an only marginally predictable system. The other is that the Indian monsoon is highly sensitive to the details of tropical east Pacific sea surface warming. It is widely believed that El Niño's impact on the Indian monsoon is through the east-west displacement of the ascending and descending branches of the Walker circulation that link Indo-Pacific climates (*9*, *10*). Unusually warm waters during El Niño cause an increased ascent associated with increased rainfall. Mass continuity requires increased descent broadly over south east Asia, suppressing monsoon rains. The hypothesis we explore is that the strength and position of these branches vary coherently with the details of El Niño warming.

We begin by examining the 23 strong El Niño years for atmosphere and ocean conditions that distinguish the 10 Indian monsoon droughts (red asterisks in Fig. 1) from the 13 drought-free years (green asterisks in Fig. 1). Figure 2A illustrates their contrasting sea surface temperatures. The most notable difference in the tropical Pacific SSTs is the greater central Pacific warming during failed Indian monsoon years (Fig. 2A). These analyses suggest India to be more prone to drought when the ocean warming signature of El Niño extends westward. Figure 2B displays the difference in tropical rainfall for the drought versus drought-free El Niño years. Though based on a smaller sample of cases for which satellite rainfall estimates are available, a physical consistency with the underlying SST anomalies in Fig. 2A is apparent. Increased rainfall occurs over the enhanced warmth of central Pacific Ocean waters, and the satellite estimates confirm dryness over India, the Indian Ocean, and other portions of Southeast Asia, indicating a wide reach to the drought signal. These rainfall anomalies form a dynamical couple that is linked via an Indo-Pacific anomalous Walker circulation, as seen in the velocity potential (*8*) at 200 hPa (Fig. 2B, contours).

The composite anomaly differences highlighted by shading in Fig. 2, A and B, are statistically significant (*8*) and are physically consistent with the expected rainfall-SST relationship. This is further seen by the separability of the probability density functions (PDFS) (*8*) of rainfall for drought versus drought-free years (Fig. 2C). While this empirical analysis does not establish causal linkages, it does suggest the hypothesis that the two flavors of El Niño (*11*) orchestrate significantly different responses in the Indian monsoon. The SST patterns of these two flavors can be described by a linear combination of the two leading, preferred patterns of tropical Pacific SST variability of the last half century (*8*), shown in Fig. 3. The first leading pattern (Fig. 3A) represents the overall strength of the ENSO events and its associated temporal pattern is highly correlated with fluctuations in the NINO3 index (Fig. 3C). The second pattern (Fig. 3B) has polarity of opposite sign between the tropical Central and Eastern Pacific and its temporal pattern is highly correlated with fluctuations of an index that measures the SST gradient across the Pacific basin (*8*) (Fig. 3D). We note in particular that the second leading pattern closely resembles the SST difference between severe drought and drought-free monsoon years (Fig. 2A, shaded).

General circulation model experiments (*8*), forced with SST patterns resulting from linear combinations of the first two leading patterns of tropical Pacific SST variability are used to test the hypothesis that "westward shifted" Pacific Ocean warm events drive more intense sinking over the Indian region, initiating severe drought. Using NCAR-CCM3, four ensemble sets of experiments are performed: (i) a 150-year control run of the GCM forced by monthly evolving global climatological mean SST; (ii) a fixed SST pattern resulting from the addition of the first two leading tropical Pacific SST patterns superimposed on the monthly evolving climatological SSTs globally; (iii) same as (ii) but by subtracting the second leading tropical Pacific SST pattern from the first; and (iv) an SST pattern corresponding to the first leading pattern (i.e., Fig. 3A) alone. The model experiments for (ii), (iii), and (iv) are performed for a range of imposed SST warmth from 0 to +3 standard deviations (SD), with results available at an interval of 0.2 SD. 10-members with different atmospheric initial conditions are analyzed for each of these incremental warmings. Climatological SSTs were prescribed outside the tropical Pacific in these experiments.

Figure 4 illustrates two key aspects of the SST forcing of our atmospheric general circulation model that mimic the empirically derived patterns of Fig. 2. Contours in Fig. 4A are analogous to the amplitude and structure of the composite El Niño SSTs for drought-free years, and correspond to the +2 SD experiment (iii) described above. Shading in Fig. 4A is analogous to the observed SST structure that discriminates severe drought from drought-free El Niño years, and corresponds to the difference between the +2 SD SST forcings of experiments (ii) and (iii). The ensemble mean rainfall and 200 hPa velocity potential difference between experiments (ii) and (iii) are shown in Fig. 4B. Notice a large-scale enhanced drought over the Indian region consistent with enhanced subsidence and vice versa in the tropical central Pacific. The similarity of this figure to that noted from the observations (Fig. 2B) is striking. This supports the hypothesis that it is the "westward shifted" El Niño events that weaken the Indian monsoon severely.

The behavior of Indian monsoon rainfall under climatological sea surface temperature conditions (control) and also under the anomalous conditions described by the three different SST patterns of experiments ii, iii and iv is assessed through the construction of PDFs (*8*) that sample all the realizations of Indian rainfall drawn from the separate members of the GCM experiments (Fig. 4C).

The PDFs of the experiments using moderate SST warming are not separated, and mean Indian rainfall is only slightly less than the control experiment. For the stronger warming, however, the PDFs of the simulated rainfall are well separated and the median rainfall values are far below those of the control experiment. Under the influence of stronger SST forcing, the PDFs of the experiments that correspond to summing and differencing the two leading tropical Pacific SST patterns fall on the dry and wet side of the median rainfall from the experiment using only the leading SST pattern, respectively. This indicates that the leading SST pattern in itself produces droughts in India when of sufficient amplitude, but depending on the sign of the superposed second leading SST pattern, the droughts in India are either strong or weak, with a clear separation in the PDFs.

Identical experiments using two other climate models yield similar results (fig. S1). Also, experiments using the actual SST difference of Fig. 2A (*8*) reproduce the results based on using the idealized SST forcings (fig. S2). It should be noted that for all SST forcings, the PDFs of monsoon rainfall (Fig. 4C) are not sharply peaked but involve a considerable range of possible outcomes. Note that the rainfall spreads are not materially different for the unforced control experiments compared to the strongly forced runs. This illustrates the influence of omnipresent internal atmospheric variability, though such in situ variability alone appears to be insufficient to generate severe monsoon failure.

The simulations demonstrate a strong dependence of the Indian monsoon on the tropical Pacific SST anomaly pattern associated with different El Niños. These results do not rule out an independent role for the Indian Ocean, as suggested in other studies (*12*–*14*) or in combination with ENSO (*15*) . Regarding the mechanism by which the “two flavors of El Niño” yield different monsoon impacts, our study has only suggested one candidate, namely a sensitivity of the tropical Walker circulation. The role of other plausible mechanisms, such as El Niño–monsoon teleconnections from the extratropics (*16*), or the role of reorganized weather disturbances, require further investigation.

The fact that the spatial configuration of tropical Pacific SST anomalies has a significant impact on the Indian monsoon indicates that traditional monsoon forecast methods using predictors that essentially capture the ENSO’s strength are likely to be unsuccessful (*17*), in years when the spatial configuration of the SST anomalies is inconsistent with its strength; 1997, 2002 and 2004 are some of the recent years that attest to this. Incorporation of SST configuration information in the statistical models should improve monsoon forecast skill (fig. S3). There is also the intriguing question of whether either of these flavors of tropical Pacific warmings will become preferred as a consequence of the ocean’s response to human-induced changes in Earth’s atmosphere’s chemical composition. Whereas the consensus of climate change models points to a so-called El Niño–like warming pattern of the tropical Pacific (*18*), the results of this study indicate that details of that human-induced ocean warming could have material consequences for the monsoon intensity over India.

References and Notes

1. K. Krishna Kumar, K. Rupa Kumar, R. G. Ashrit, N. R. Deshpande, J. W. Hansen, *Int. J. Climatol.* **24**, 1375 (2004).
2. S. G. Philander, *Our Affair with El Niño* (Princeton Univ. Press, (2004).
3. S. Gadgil *et al., Curr. Sci.* **83**, 394 (2002).
4. S. Gadgil, M. Rajeevan, R. Nanjundiah, *Curr. Sci.* **88**, 1389 (2005).
5. S. Hastenrath, *Climate Dynamics of the Tropics* (Kluwer Academic Publishers, Dordrecht, The Netherlands, 1991).
6. K. Krishna Kumar, M. K. Soman, K. Rupa Kumar, *Weather* **50**, 449 (1995).
7. J. Shukla, D. A. Paolino, *Mon. Weather Rev.* **111**, 1830 (1983).
8. Materials and methods are available as supporting material on *Science* Online.
9. J. Shukla, in *Monsoons*, J. S. Fein, P. L. Stephens, Eds. (Wiley, New York, 1987), p. 399.
10. C. F. Ropelewski, M. S. Halpert, *Mon. Weather Rev.* **115**, 1606 (1987).
11. K. Trenberth, *Proc. 18th Ann. Clim. Diagnost. Workshop*, Boulder, CO, 50 (1993).
12. N. H. Saji, B. N. Goswamy, P. N. Vinayachandran, T. Yamagata, *Nature* **401**, 360 (1999).
13. S. Gadgil, P. N. Vinayachandran, P. A. Francis, S. Gadgil, *Geophys. Res. Lett.* **31**, GL12213 (2004).
14. K. Krishna Kumar, M. Hoerling, B. Rajagopalan, *Geophys. Res. Lett.* **32**, GL08704 (2005).
15. H. Annamalai, P. Liu, *Q. J. R. Meteorol. Soc.* **131**, 805 (2005).
16. B. N. Goswami, P. K. Xavier, *Geophys. Res. Lett.* **32**, GL023216 (2005).
17. K. Krishna Kumar, B. Rajagopalan, M. Cane, *Science* **284**, 2156 (1999).
18. M. Cane *et al*., *Science* **275**, 957(1997); IPCC, *Climate Change 2001: The Scientific Basis: Summary for Policy Makers and Technical Summary of the Working Group 1 Report* (Cambridge Univ. Press, Cambridge, 2001).

19. The first author thankfully acknowledges the funding support from CIRES and APN. Funding provided to the third author by NOAA’s Office of Global Programs is gratefully acknowledged. We also thank T. Xu and J. Eischeid for their contributions.

Supporting Online Material

www.sciencemag.org/cgi/content/full/1131152/DC1
Materials and Methods
Figs. S1 to S3

12 June 2006; accepted 29 August 2006
Published online 7 September 2006;10.1126/science.1131152
Include this information when citing this paper

Fig 1. Plot of standardized, All Indian summer June to September (JJAS) monsoon rainfall and summer NINO3 anomaly index. Severe drought and drought-free years during El Niño events (standardized NINO3 anomalies > 1) are shown in red and green, respectively.

Fig 2. (**A**) Composite SST difference pattern between severe drought (shaded) and drought-free El Niño years. Composite

SST anomaly pattern of drought-free years are shown as contours. (**B**) Composite difference pattern between severe drought and drought-free years of velocity potential (contours) and rainfall (shaded). (**C**) PDF of All India Summer Monsoon Rainfall from severe-drought (red curve) and drought-free (blue curve) years associated with El Nino occurrence and, from the non-ENSO years (green curve). SST and velocity potential composite differences are based on 1950 to 2004 period, rainfall composites are based on 1979 to 2004 period and the PDFs are based on 1873 to 2004 period.

Fig 3. (**A**) The first leading pattern of the tropical Pacific SST variability. (**B**) Same as (A) but for the second leading pattern. (**C**) The first leading temporal pattern (black line) overlaid with the monthly NINO3 index (red line). (**D**) The second leading temporal pattern (black line) overlaid with the TNI index (red line).

Fig 4. (**A**) Contours are of the +2 SD experiment (iii) and are analogous to the amplitude and structure of the composite El Niño SSTs for drought-free years in Fig. 2A. Shadings are of the difference between the +2 SD SST forcings of experiments (ii) and (iii) and are analogous to the observed SST structure that discriminates severe drought from drought-free El Niño years. (**B**) The ensemble mean rainfall (shading) and 200 hPa velocity potential (contour) differences between experiments (ii) and (iii). (**C**) The PDF of the Indian monsoon rainfall corresponding to the control (i.e., unforced) experiment (i) (top, green curve), corresponding to the forced experiments (ii; red curve), (iii; blue curve) and (iv; dashed line) with +1 SD (middle) and +2 SD (bottom) imposed SST anomalies. For forced experiment (iv) only the median value (dashed line) is shown. For the forced experiments each PDF is estimated from 30 ensembles. The model rainfall has been averaged over the Indian monsoon region of 8°N-30°N, 70°E-90°E. See text for detailed descriptions of the SST anomalies used in experiments (i) to (iv).

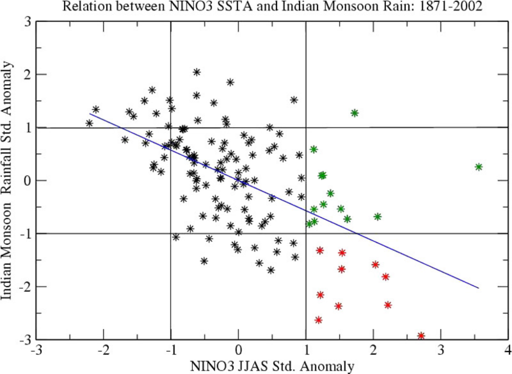

Relation between NINO3 SSTA and Indian Monsoon Rain: 1871-2002
Indian Monsoon Rainfall Std. Anomaly
NINO3 JJAS Std. Anomaly
3
2
1
0
-1
-2
-3
-3
-2
-1
0
1
2
3
4

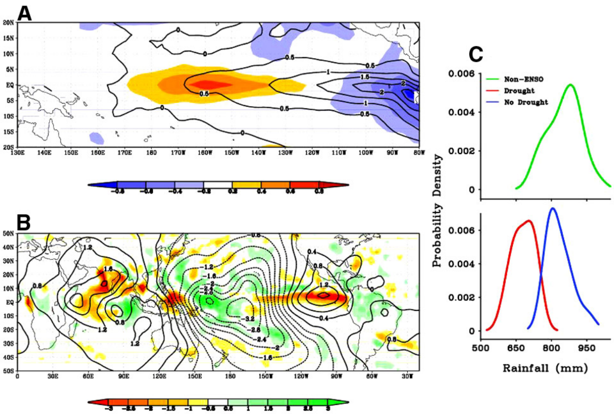
A
B
C
Non-ENSO
Drought
No Drought
Probability Density
Rainfall (mm)

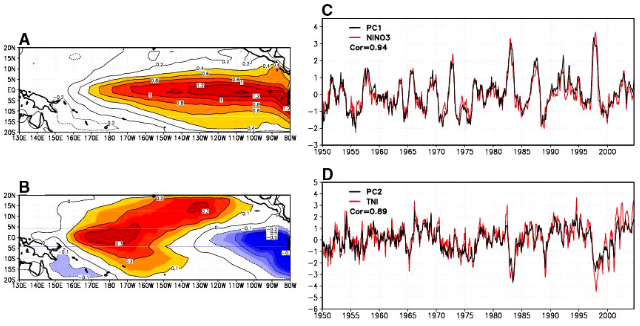

A
B
C
D
PC1
NINO3
Cor=0.94
PC2
TNI
Cor=0.89

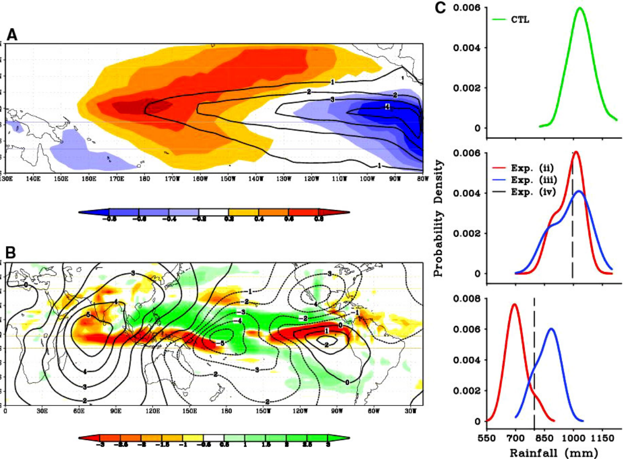

A
20N 15N 10N 5N EQ 5S 10S 15S 20S
130E 140E 150E 160E 170E 180 170W 160W 150W 140W 130W 120W 110W 100W 90W 80W
-0.8 -0.6 -0.4 -0.2 0.2 0.4 0.6 0.8
B
50N 40N 30N 20N 10N EQ 10S 20S 30S 40S 50S
0 30E 60E 90E 120E 150E 180 150W 120W 90W 60W 30W
-3 -2.5 -2 -1.5 -1 -0.5 0.5 1 1.5 2 2.5 3
C
CTL
Exp. (ii)
Exp. (iii)
Exp. (iv)
Probability Density
Rainfall (mm)
550 700 850 1000 1150